# Self-consistent collective coordinate for reaction path and inertial mass

Kai Wen[1,*] and Takashi Nakatsukasa[1,2]
[1]*Center for Computational Sciences and Faculty of Pure and Applied Sciences, University of Tsukuba, Tsukuba 305-8577, Japan*
[2]*RIKEN Nishina Center, Wako 351-0198, Japan*
(Received 10 August 2016; published 21 November 2016)

We propose a numerical method to determine the optimal collective reaction path for a nucleus-nucleus collision, based on the adiabatic self-consistent collective coordinate (ASCC) method. We use an iterative method, combining the imaginary-time evolution and the finite amplitude method, for the solution of the ASCC coupled equations. It is applied to the simplest case, $\alpha$-$\alpha$ scattering. We determine the collective path, the potential, and the inertial mass. The results are compared with other methods, such as the constrained Hartree-Fock method, Inglis's cranking formula, and the adiabatic time-dependent Hartree-Fock (ATDHF) method.

DOI: 10.1103/PhysRevC.94.054618

## I. INTRODUCTION

The time-dependent Hartree-Fock (TDHF) method has been extensively applied to studies of heavy-ion reactions [1–5]. The TDHF method provides a successful description for the time evolution of one-body observables. Its small-amplitude limit corresponds to the random-phase approximation [6,7], which is a current leading theory for nuclear response calculations. However, beyond the linear regime, it is not trivial to extract quantum mechanical information from the TDHF trajectories of given initial values. It is also well known that the TDHF method has some drawbacks due to its semiclassical nature [1,6]. For instance, the real-time description of sub-barrier fusion and spontaneous fission processes is practically impossible, because a single Slater determinant with a single average mean-field potential is not capable of describing quantum mechanical processes in rare channels.

The "requantization" of TDHF is a possible solution to these problems, that was proposed from a viewpoint of the path integral [1,8]. However, the original quantization prescription requires the identification of periodic TDHF trajectories, which is a very difficult task. As far as we know, there has been no application of the theory to realistic nuclear problems [9]. A family of the periodic TDHF trajectories is associated with a collective subspace decoupled from the other intrinsic degrees of freedom. If we identify the collective subspace spanned by a small number of canonical variables, the requantization becomes much easier than finding the periodic orbits [3]. In fact, the theory of the adiabatic TDHF (ATDHF) method aimed to determine such an optimum collective subspace [10–13]. The ATDHF, however, encounters a "nonuniqueness" problem; namely it cannot provide a unique solution for the collective subspace. In order to uniquely fix the solution, a prescription, so-called validity condition, was proposed [14]. Goeke, Reinhard, and coworkers have developed a numerical recipe for the reaction path and inertial mass, solving the ATDHF equations of the initial-value problem [15,16]. Their procedure requires us to calculate a large number of trajectories with different initial states, then to obtain the optimal collective path as an envelope curve of those [15].

The self-consistent collective coordinate (SCC) method, originally proposed by Marumori and coworkers [17], is solely based on the invariance principle of the TDHF equation in the collective subspace, which treats the collective coordinate $q$ and the momentum $p$ on an equal footing. The SCC method is able to determine the unique collective path. In addition, the Anderson-Nambu-Goldstone (ANG) modes are properly decoupled in the SCC method [3,18]. Its weak point is that practical solutions to the basic equation were restricted to a perturbative expansion around the HF state. To overcome this perturbative nature of the SCC, a method treating the coordinate $q$ in a nonperturbative way but expanding with respect to momenta $p$ was later proposed. It is named the "adiabatic self-consistent collective coordinate (ASCC) method" [19]. The ASCC method provides an alternative practical solution to SCC [19]: The state is determined at each value of $q$ by solving the equation expanded up to the second order in $p$. The ASCC method has been successfully applied to nuclear structure problems with large-amplitude shape fluctuations and/or oscillations for the Hamiltonian of the separable interactions [3,20–26]. It should be noted that a solution to the nonuniqueness problem of the ATDHF method was given by higher-order equations with respect to momenta [27,28], which are similar to the ASCC equations.

In this paper, we apply the ASCC method to nuclear reaction studies, then self-consistently determine the optimal reaction path, the internuclear potential, and the inertial mass. Since the separable interactions, such as the pairing-plus-quadrupole interaction, are not applicable to a system with two colliding nuclei, we need to treat a Hamiltonian of nonseparable type. For this purpose, we developed a computer code employing a novel numerical technique. We use a procedure combining the imaginary-time method [29] and the finite-amplitude method [30–32] for the solution of the ASCC equations. We show that this method nicely works for the three-dimensional (3D) coordinate-space representation, taking a reaction of $^{8}\mathrm{Be} \leftrightarrow \alpha + \alpha$ as an example.

The paper is organized as follows. In Sec. II, we give the formulation of the basic ASCC equations to determine the one-dimensional (1D) collective path and the canonical

*wenkai@nucl.ph.tsukuba.ac.jp

 

variables $(q,p)$. In Sec. III, we show the numerical results and compare with those of conventional methods. A summary and concluding remarks are given in Sec. IV.

## II. THEORETICAL FRAMEWORK

### A. The adiabatic self-consistent collective coordinate (ASCC) method

The SCC method aims to determine a collective submanifold embedded in the large dimensional TDHF space of Slater determinants, which is maximally decoupled from the remaining intrinsic degrees of freedom. For the 1D collective path, a pair of canonical variables $(q,p)$ along the collective path are introduced by labeling the Slater determinants as $|\psi(p,q)\rangle$, where $q$ and $p$ respectively represent the coordinate and the conjugate momentum. Once the states $|\psi(q,p)\rangle$ are determined, the (classical) collective Hamiltonian is given by $\mathcal{H}_{\rm coll}(q,p) \equiv \langle\psi(q,p)|\hat{H}|\psi(q,p)\rangle$, where $\hat{H}$ is the total Hamiltonian of the system. Therefore, the main task is to determine $|\psi(q,p)\rangle$ on a decoupled collective submanifold.

In the ASCC [19], the wave function is written in the form

$$|\psi(p,q)\rangle = e^{ip\hat{Q}(q)}|\psi(q)\rangle, \tag{1}$$

using a local generator $\hat{Q}(q)$ which is defined as

$$\hat{Q}(q)|\psi(q)\rangle = -i\partial_p|\psi(q)\rangle|_{p=0}. \tag{2}$$

The collective coordinate operator $\hat{Q}(q)$ is an infinitesimal generator for "accelerating" the system. The momentum operator is introduced in a similar way as an infinitesimal generator for "translating" the system, $\hat{P}(q)|\psi(q)\rangle = i\partial_q|\psi(q)\rangle$.

Since the Thouless theorem guarantees that small variation of a Slater determinant can be generated by the particle-hole (ph) excitations [6], the local generators, $\hat{Q}(q)$ and $\hat{P}(q)$, can be written in terms of ph and hp operators as

$$\hat{P}(q) = i\sum_{n,j} P_{nj}(q)a_n^\dagger(q)a_j(q) + \text{H.c.}, \tag{3}$$

$$\hat{Q}(q) = \sum_{n,j} Q_{nj}(q)a_n^\dagger(q)a_j(q) + \text{H.c.} \tag{4}$$

In this paper, the indexes $i,j$ and $n,m$ refer to the hole and particle states with respect to $|\phi(q)\rangle$, respectively, Hereafter, the creation and annihilation operators are denoted as $(a_n^\dagger,a_i)$ instead of $(a_n^\dagger(q),a_i(q))$ for simplicity. These generators are required to follow the weak canonicity condition

$$\langle\psi(q)|[i\hat{P}(q),\hat{Q}(q)]|\psi(q)\rangle = 1. \tag{5}$$

In the ASCC, the collective momentum $p$ is assumed to be small. Keeping the expansion with respect to $p$ up to the second order, the invariance principle of the TDHF equation leads to a set of ASCC equations [3,4,19,20,22,33] to determine the wave function $|\psi(q)\rangle$ and the local generators $(\hat{P}(q),\hat{Q}(q))$ self-consistently along the collective path. In this paper, we consider only the 1D collective motion, without taking the pairing correlations into account. The equations in the zeroth, first, and second order in momentum read, respectively,

$$\delta\langle\psi(q)|\hat{H}_{\rm mv}(q)|\psi(q)\rangle = 0 \tag{6}$$

$$\delta\langle\psi(q)|\left[\hat{H}_{\rm mv}(q),\frac{1}{i}\hat{P}(q)\right] - \frac{\partial^2 V}{\partial q^2}\hat{Q}(q)|\psi(q)\rangle = 0, \tag{7}$$

$$\delta\langle\psi(q)|[\hat{H}_{\rm mv}(q),i\hat{Q}(q)] - \frac{1}{M(q)}\hat{P}(q)|\psi(q)\rangle = 0, \tag{8}$$

where $\hat{H}_{\rm mv}(q) \equiv \hat{H} - (\partial V/\partial q)\hat{Q}(q)$ is the "moving" Hamiltonian. The collective potential $V(q)$ is defined as

$$V(q) = \langle\psi(q)|\hat{H}|\psi(q)\rangle, \tag{9}$$

and $M(q)$ is the inertial mass of the collective motion. Equation (6) is called the moving mean-field equation [or moving Hartree-Fock (HF) equation], and Eqs. (7) and (8) are the moving random-phase approximation (RPA).

In fact, to derive the second-order equation (8), an additional term called the curvature term [19] is neglected. Although the exact treatment of the curvature term is possible, it involves numerically iterative tasks and has only minor effect on the final result [33]. Here, we neglect this curvature term, which leads to Eq. (8). Equation (6) looks similar to a constrained Hartree-Fock (CHF) equation. However, the constraint operator $\hat{Q}(q)$ changes along the collective path $|\psi(q)\rangle$, which is self-consistently determined by the moving RPA equations (7) and (8).

Substituting $\hat{P}$ and $\hat{Q}$ of Eqs. (3) and (4) into Eqs. (7) and (8) leads to

$$\begin{pmatrix} A(q) & B(q) \\ B^*(q) & A^*(q) \end{pmatrix}\begin{pmatrix} P(q) \\ P^*(q) \end{pmatrix} = \frac{\partial^2 V}{\partial q^2}\begin{pmatrix} Q(q) \\ Q^*(q) \end{pmatrix}, \tag{10}$$

$$\begin{pmatrix} A(q) & B(q) \\ B^*(q) & A^*(q) \end{pmatrix}\begin{pmatrix} Q(q) \\ -Q^*(q) \end{pmatrix} = \frac{1}{M(q)}\begin{pmatrix} P(q) \\ -P^*(q) \end{pmatrix}, \tag{11}$$

where the $A$ and $B$ matrix elements are defined as

$$\begin{aligned} A_{minj}(q) &= \langle\psi(q)|a_i^\dagger a_m[\hat{H}_{\rm mv}(q),a_n^\dagger a_j]|\psi(q)\rangle, \\ B_{minj}(q) &= -\langle\psi(q)|a_i^\dagger a_m[\hat{H}_{\rm mv}(q),a_j^\dagger a_n]|\psi(q)\rangle. \end{aligned} \tag{12}$$

When all of these matrix elements are real, Eqs. (10) and (11) can be recast into an eigenvalue equation

$$\{A(q)+B(q)\}\{A(q)-B(q)\}Q(q) = \omega^2(q)Q(q), \tag{13}$$

with

$$\omega^2(q) = \frac{1}{M(q)}\frac{\partial^2 V}{\partial q^2}, \tag{14}$$

where $\omega(q)$ is the moving-RPA eigenfrequency. $\omega(q)$ can be purely imaginary ($\omega^2(q) < 0$). The generator $\hat{P}(q)$ can be obtained from a matrix equation for $P_{nj}(q)$,

$$P(q) = M(q)\{A(q)-B(q)\}Q(q). \tag{15}$$

Equation (13) has many solutions, among which we choose the collective mode of our interest. For instance, in the numerical calculation for the scattering $\alpha+\alpha \leftrightarrow {}^8$Be in Sec. III, the lowest quadrupole mode of excitation is selected.

Since the scale of the coordinate is arbitrary, the ASCC equations (6), (7), and (8) and the weak canonicity condition (5) are invariant with respect to the scale transformation

of the collective coordinate, $q \to \alpha q$ ($p \to p/\alpha$). The generators and the collective inertial mass are transformed as $\hat{Q}(q) \to \alpha \hat{Q}(q)$, $\hat{P}(q) \to \hat{P}(q)/\alpha$, and $M(q) \to \alpha^{-2} M(q)$, respectively. Therefore, when we perform the numerical calculation to determine the collective coordinate $q$, we need a condition to fix the scale of the coordinate $q$. A convenient choice could be the condition that the mass $M(q)$ is unity, which we adopt in the present paper. Then, the eigenvalue $\omega^2$ of Eq. (13) gives the second derivative of $V(q)$ with respect to $q$.

In this way, we obtain a series of states $|\psi(q)\rangle$ on the collective path, the collective potential $V(q)$ of Eq. (9), and the collective inertial mass $M(q)$ equal to unity by tuning the scale of $q$. Thus, the collective Hamiltonian is constructed as

$$\mathcal{H}_{\rm coll} = \tfrac{1}{2}\dot{q}^2 + V(q). \tag{16}$$

The canonical quantization of this Hamiltonian immediately leads to

$$\hat{H}_{\rm coll} = -\frac{1}{2}\left(\frac{d}{dq}\right)^2 + V(q). \tag{17}$$

### B. Mapping to different variables

In order to obtain a physical picture of the collective dynamics, it is often convenient to adopt an "intuitive" variable, such as the distance between two nuclei, $R$. Of course, the optimal collective coordinate $q$, determined by the ASCC solutions, is different from $R$, in general. Nevertheless, as far as the one-to-one correspondence between $q$ and $R$ is guaranteed, we may use the variable $R = R(q)$ to modify the scale of the coordinate. Without affecting the collective dynamics, the collective Hamiltonian, Eqs. (16) and (17), is rewritten in terms of $R$.

Let us denote a new variable as $R$, defined by the expectation value of the corresponding one-body Hermitian operator $\hat{R}$. For instance, the operator of the relative distance between two symmetric nuclei ($2 \times A/2$) is given by

$$\hat{R} \equiv \frac{1}{A/2}\int d\vec{r}\, \hat{\psi}^\dagger(\vec{r})\hat{\psi}(\vec{r})\{z\theta(z) - z\theta(-z)\}, \tag{18}$$

where $\theta(z)$ is the step function. We also assume the one-to-one mapping between $q$ and $R$, $R(q) = \langle\psi(q)|\hat{R}|\psi(q)\rangle$ and its inverse function $q(R)$. The transformation of the collective potential, $V(q) \to V(R)$, is trivial: $V(R) = V(q(R))$. In contrast, the inertial mass is transformed as

$$M(R) = M(q)\left(\frac{dq}{dR}\right)^2 = \left(\frac{dq}{dR}\right)^2 = \left(\frac{dR}{dq}\right)^{-2}, \tag{19}$$

where we use $M(q) = 1$. The inertial mass $M(R)$ is not constant but depends on $R$. The collective Hamiltonian is rewritten as

$$\mathcal{H}^R_{\rm coll} = \tfrac{1}{2}M(R)\dot{R}^2 + V(R). \tag{20}$$

A quantization identical to Eq. (17) is given by the Pauli prescription [34]

$$\hat{H}^R_{\rm coll} = -\frac{1}{2}\frac{1}{\sqrt{M(R)}}\frac{d}{dR}\frac{1}{\sqrt{M(R)}}\frac{d}{dR} + V(R). \tag{21}$$

The mass $M(R)$ requires calculation of the derivative, $dR/dq$ or $dq/dR$, in Eq. (19). These quantities can be obtained by use of the local generator $\hat{P}(q)$,

$$\frac{dR}{dq} = \frac{d}{dq}\langle\psi(q)|\hat{R}|\psi(q)\rangle = \langle\psi(q)|\left[\hat{R}, \frac{1}{i}\hat{P}(q)\right]|\psi(q)\rangle$$
$$= 2\sum_{mi} R_{mi}(q)P_{mi}(q), \tag{22}$$

where $R_{mi}(q)$ are the ph matrix elements of $\hat{R}$ with respect to the state $|\psi(q)\rangle$ and are assumed to be real. Since this calculation can be performed using the local quantities at $q$, it has an advantage over the conventional finite difference, $dR/dq \approx \{R(q+\delta q) - R(q)\}/\delta q$, with two adjacent points, $|\psi(q)\rangle$ and $|\psi(q+\delta q)\rangle$, on the collective path. Thus, we use Eq. (22) for calculation of the derivatives.

In the present ASCC method, the variable $R$ is merely a parameter to represent the collective coordinate $q = q(R)$. It should be emphasized that this is different from assuming the collective coordinate to be $R$. First of all, the potential is different, $V(R) = \langle\psi(q(R))|H|\psi(q(R))\rangle \neq \langle\phi(R)|H|\phi(R)\rangle$. Here, $|\phi(R)\rangle$ is calculated by minimization of the total energy with a constraint on $R$. Even if the state $|\phi(R)\rangle$ is close to $|\psi(q(R))\rangle$, the inertial masses $M^R(R)$ for the motion along the direction $R$ can be very different from $M(R)$. The ASCC method guarantees a block-diagonal form of the inertial tensor between the collective coordinate $q$ and the rest of intrinsic degrees $\{\vec{\xi}\}$ perpendicular to $q$. In contrast, the inertial mass tensor $M^R(R)$ for the coordinate $R$ is not block-diagonal in general. Thus, we need to adopt its diagonal element $M^R(R)$, which is different from $M(R)$:

$$M^R(R) - M(R) = \sum_{ij}\mathcal{M}_{ij}(q(R))\frac{d\xi^i}{dR}\frac{d\xi^j}{dR}, \tag{23}$$

where $\mathcal{M}_{ij}(q(R))$ is the inertial mass tensor for the intrinsic motion. Last but not least, the inertial mass $M^R(R)$ is usually calculated according to Inglis's cranking formula, $M^R_{\rm cr}(R)$ (see Sec. III C 1). The cranking mass $M^R_{\rm cr}(R)$ cannot take into account the effects of the time-odd mean fields. In contrast, the ASCC inertial mass $M(R)$, which is determined from the moving RPA equation (8), reflects the presence of the time-odd mean fields. Therefore, even if the collective coordinates $q$ and $R$ are identical, the calculated inertial masses may be different. For instance, for the translational (center-of-mass) motion of the nucleus, the cranking mass fails to reproduce the total mass, $M^R_{\rm cr}(R) \neq Am$, when the effective mass $m^*$ is different from the bare nucleon mass $m$. It is compensated by the time-odd effect in the ASCC inertial mass, that leads to the exact relation $M(R) = Am$.

### C. Numerical algorithm and details

#### 1. Coordinate-space and mixed representation

In this paper, we adopt the Bonche-Koonin-Negele (BKN) energy density functional [35] for the Hamiltonian $\hat{H}$.[1]

[1]The diagonal approximation of the center-of-mass energy modifies the nucleon mass, $m^{-1} \to m^{-1}(1 - A^{-1})$. In this paper, we do not adopt this correction, thus the nucleon mass is the bare mass.

The BKN energy density functional assumes spin-isospin symmetry without the spin-orbit interaction, thus all the single-particle states at the HF ground state are real [$\varphi_i^*(\vec{r}) = \varphi_i(\vec{r})$]. The one-body Hamiltonian is given by

$$h[\rho] = -\frac{1}{2m}\nabla^2 + \frac{3}{4}t_0\rho(\vec{r}) + \frac{3}{16}t_3\rho^2(\vec{r}) + \int d\vec{r}' v(\vec{r}-\vec{r}')\rho(\vec{r}'), \tag{24}$$

where $v(\vec{r})$ is the sum of the Yukawa and the Coulomb potentials,

$$v(\vec{r}) \equiv V_0 a\frac{e^{-r/a}}{r} + \frac{(e/2)^2}{r}. \tag{25}$$

We take the same parameter set as in Ref. [35].

For the BKN energy density functional, it is convenient to utilize the coordinate-space representation. Each single-particle wave function $\varphi_i(\vec{r})$ is represented in the 3D grid points of a square mesh, $\varphi_{\vec{k}i} \equiv \varphi_i(\vec{r}_{\vec{k}})$ with $\vec{r}_{\vec{k}} = \vec{k} \times h = (k_x, k_y, k_z) \times h$, where $h$ is the mesh size. Although every quantity is defined locally at $q$, in this subsection we omit the collective coordinate $q$ for simplicity, e.g., $\varphi_i(\vec{r};q) \to \varphi_i(\vec{r})$. The 3D space is a rectangular box of volume $10 \times 10 \times 16$ fm$^3$ with mesh size $h = 0.8$ fm.

We adopt the mixed representation for the moving RPA equation: The particle-state indices $m,n,\ldots$ are replaced by the coordinate $\vec{r}$. Thus, the generator $\hat{Q}$ of Eq. (4) is represented as

$$\hat{Q} = \int d\vec{r} \sum_j Q_j(\vec{r})a^\dagger(\vec{r})a_j + \text{H.c.} \approx h^3 \sum_{\vec{k}}\sum_j Q_{\vec{k},j}a_{\vec{k}}^\dagger a_j + \text{H.c.}, \tag{26}$$

where $Q_{\vec{k},j} = Q_j(\vec{r}_{\vec{k}})$ and $a_{\vec{k}}^\dagger \equiv a^\dagger(\vec{r}_{\vec{k}})$. Since the coordinate indices $\vec{r}_{\vec{k}}$ contain not only the particle states but also hole states, we should remove the hole parts. Using the projection operator, $\hat{C} \equiv 1 - \sum_i |\varphi_i\rangle\langle\varphi_i|$, this is done by replacing $Q_j(\vec{r}) = \langle\vec{r}|Q_j\rangle$ by

$$\int d\vec{r}' C(\vec{r},\vec{r}')Q_j(\vec{r}') = Q_j(\vec{r}) - \sum_i \varphi_i(\vec{r})\langle\varphi_i|Q_j\rangle, \tag{27}$$

where $C(\vec{r},\vec{r}') \equiv \delta(\vec{r}-\vec{r}') - \sum_i \varphi_i(\vec{r})\varphi_i^*(\vec{r}')$. Equivalently, $|Q_j\rangle$ is replaced by $\hat{C}|Q_j\rangle$. Similar modification is performed for the generator $\hat{P}$ of Eq. (3).

The matrices of Eq. (12) are represented as $A_{\vec{k}i\vec{k}'j} = A_{ij}(\vec{r}_{\vec{k}},\vec{r}_{\vec{k}'})$, and the same for matrix $B$. The hole contributions are removed in the same manner as in Eq. (27). For instance, $(A\cdot Q)_{mi} = \sum_{nj} A_{minj}Q_{nj}$ in the ph representation becomes

$$(A\cdot Q)_i(\vec{r}) = \sum_j \iiint d\vec{r}_1 d\vec{r}_2 d\vec{r}_3 \times C(\vec{r},\vec{r}_1)A_{ij}(\vec{r}_1,\vec{r}_2)C(\vec{r}_2,\vec{r}_3)Q_j(\vec{r}_3), \tag{28}$$

which can be discretized as

$$(A\cdot Q)_{\vec{k}i} = h^9 \sum_j \sum_{\vec{k}_1\vec{k}_2\vec{k}_3} C_{\vec{k}\vec{k}_1}A_{\vec{k}_1i\vec{k}_2j}C_{\vec{k}_2\vec{k}_3}Q_{\vec{k}_3j}, \tag{29}$$

where $C_{\vec{k}_1\vec{k}_2} \equiv h^{-3}\delta_{\vec{k}_1\vec{k}_2} - \sum_i \varphi_{\vec{k}_1 i}\varphi_{\vec{k}_2 i}^*$.

Although we remove the hole-hole contributions in this manner, the RPA matrices are oversize and contain redundant components. Therefore, the diagonalization of the moving RPA equation produces spurious solutions that consist of only hole-hole elements.[2] The number of these spurious modes is equal to square of the number of the hole orbits, $A^2$. These spurious solutions are decoupled and have no influence on physical solutions. Thus, we simply discard the spurious solutions after the diagonalization of the RPA matrix.

#### 2. *Finite amplitude method for the moving RPA solution*

Solutions of the moving RPA equation (13) determine the local generators $\hat{Q}(q)$, then $\hat{P}(q)$ is obtained from Eq. (15). To evaluate the matrix elements of $A \pm B$ in Eq. (13), we adopt the finite amplitude method (FAM) [30–32,36–41], especially the matrix FAM (m-FAM) prescription [32]. The FAM requires only the calculations of the single-particle Hamiltonian constructed with independent bra and ket states [30], providing us an efficient tool to solve the RPA problem.

Let us assume that the state $|\psi(q)\rangle$ is determined from the moving HF equation (6). The single-particle states $|\varphi_i(q)\rangle$ and their energies $\epsilon_i(q)$ of the hole states are defined by

$$\hat{h}_{\rm mv}(q)|\varphi_i(q)\rangle = \epsilon_i(q)|\varphi_i(q)\rangle, \tag{30}$$

where $h_{\rm mv}(q) = h_{\rm HF}[\rho_0(q)] - \lambda(q)\hat{Q}(q)$ is the single-particle Hamiltonian reduced from $\hat{H}_{\rm mv}(q) = \hat{H} - \lambda(q)\hat{Q}(q)$ with $\lambda(q) = \partial V/\partial q$. The self-consistent density $\rho_0(q)$ is given by $\rho_0(q) = \sum_i |\varphi_i(q)\rangle\langle\varphi_i(q)|$. According to Ref. [32], the matrix elements $(A\pm B)_{\vec{r}i,\vec{r}'j}$ can be calculated as follows:

$$(A\pm B)_{\vec{r}i,\vec{r}'j} = [h_{\rm mv}(\vec{r},\vec{r}') - \epsilon_i\delta(\vec{r}-\vec{r}')]\delta_{ij} + \delta h_{[\vec{r}i,\vec{r}'j]}. \tag{31}$$

Here, again, the $q$ dependence is omitted for simplicity. Using a small real parameter $\eta = 10^{-4}$, the m-FAM provides the elements $\delta h_{[\vec{r}i,\vec{r}'j]}$ by

$$\delta h_{[\vec{r}i,\vec{r}'j]} = \eta^{-1}\langle\vec{r}|\{h_{\rm mv}[\rho_{[\vec{r}'j]}] - h_{\rm mv}[\rho_0]\}|\varphi_i\rangle, \tag{32}$$

where $\rho_{[\vec{r}'j]}$ is defined as

$$\rho_{[\vec{r}j]} = \rho_0 + \eta\big(|\vec{r}\rangle\langle\varphi_j| + |\varphi_j\rangle\langle\vec{r}|\big). \tag{33}$$

Note that Eq. (32) requires only the operation of the single-particle Hamiltonian on the hole orbits. In addition, the single-particle Hamiltonian $h_{\rm mv}$ can be replaced by the HF single-particle Hamiltonian $h_{\rm HF}$ in Eqs. (31) and (32). It is trivial, for Eq. (32), to see that the term $\lambda\hat{Q}$ is canceled by the subtraction. For Eq. (31), this is because the hole components are always removed from $\vec{r}$ and $\vec{r}'$, and the generator $\hat{Q}$ has only ph and hp components.

#### 3. *Imaginary-time method for the moving HF solution*

Let us assume that $\hat{Q}(q)$ is determined from the moving RPA equation, and now we want to move to the next point on

[2]They should not be confused with the zero modes associated with the symmetry breaking of the state $|\psi(q)\rangle$, which are often called "spurious modes" as well.

the collective path ($q \to q + \delta q$). This can be done by solving the moving HF equation (6), with the following constraint:

$$\langle\psi(q+\delta q)|\hat{Q}(q)|\psi(q+\delta q)\rangle = \delta q, \tag{34}$$

which controls the step size of the collective coordinate $\delta q$. Equation (34) can be understood as

$$\begin{aligned}&\langle\psi(q+\delta q)|\hat{Q}(q)|\psi(q+\delta q)\rangle\\ &= \langle\psi(q)|e^{i\delta q\hat{P}(q)}\hat{Q}(q)e^{-i\delta q\hat{P}(q)}|\psi(q)\rangle\\ &\approx \delta q\langle\psi(q)|[i\hat{P}(q),\hat{Q}(q)]|\psi(q)\rangle = \delta q,\end{aligned} \tag{35}$$

by the use of the local generator $\hat{P}(q)$ and the canonicity condition (5).

Hereafter, in this subsection, the quantities without the explicit $q$ dependence are those defined at $q + \delta q$, such as $|\varphi_i\rangle = |\varphi_i(q+\delta q)\rangle$. The moving HF equation (6) is iteratively solved using the imaginary-time method [29] which is efficient in the coordinate-space representation. Each single-particle wave function is evolved as $|\varphi_i^{(n)}\rangle \to |\varphi_i^{(n+1)}\rangle = |\varphi_i^{(n)}\rangle + |\delta\varphi_i^{(n)}\rangle$, where

$$\left|\delta\varphi_i^{(n)}\right\rangle = -\epsilon\left\{h_{\rm HF}^{(n)} - \lambda^{(n)}\hat{Q}(q)\right\}\left|\varphi_i^{(n)}\right\rangle, \tag{36}$$

with a small real parameter $\epsilon > 0$. $h_{\rm HF}^{(n)}$ is the single-particle Hamiltonian calculated with the density $\hat{\rho}^{(n)} = \sum_i |\varphi_i^{(n)}\rangle\langle\varphi_i^{(n)}|$. Here we approximate $\hat{Q}(q+\delta q)$ in Eq. (6) by $\hat{Q}(q)$, provided that $\delta q$ is small enough. The Lagrange multiplier $\lambda$ is determined by the constraint (34). In the first order in $\epsilon$, $\lambda^{(n)}$ is given by

$$\begin{aligned}\lambda^{(n)} &= (\epsilon{\rm Tr}[\{\hat{Q}(q),\hat{Q}(q)\}\hat{\rho}^{(n)}])^{-1}\\ &\times\left(\delta q - {\rm Tr}[\hat{Q}(q)\hat{\rho}^{(n)}] + \epsilon{\rm Tr}\left[\left\{\hat{Q}(q),h_{\rm HF}^{(n)}\right\}\hat{\rho}^{(n)}\right]\right)\end{aligned} \tag{37}$$

at each iteration. Here, the traces are calculated as

$$\begin{aligned}{\rm Tr}[\{\hat{Q}(q),\hat{Q}(q)\}\hat{\rho}^{(n)}] &= 2\sum_j\langle Q_j(q)|\hat{\rho}^{(n)}|Q_j(q)\rangle\\ &+2\sum_{ij}\langle\varphi_i(q)|\hat{\rho}^{(n)}|\varphi_j(q)\rangle\\ &\times\langle Q_j(q)|Q_i(q)\rangle,\end{aligned} \tag{38}$$

$$\begin{aligned}{\rm Tr}[\{\hat{Q}(q),\hat{O}\}\hat{\rho}^{(n)}] &= \sum_j\langle Q_j(q)|\hat{O}\hat{\rho}^{(n)}|\varphi_j(q)\rangle\\ &+\sum_j\langle\varphi_j(q)|\hat{O}\hat{\rho}^{(n)}|Q_j(q)\rangle + {\rm c.c.},\end{aligned} \tag{39}$$

with $\hat{O} = 1$ and $h_{\rm HF}^{(n)}$. Note $|Q_j(q)\rangle = \hat{C}(q)|Q_j(q)\rangle$ with $\hat{C}(q) = 1 - \sum_i |\varphi_i(q)\rangle\langle\varphi_i(q)|$. In actual calculations, we also have constraints on the center of mass and the direction of the principal axis. These additional constraints are easily taken into account by extending Eqs. (36) and (37).

According to Eq. (6), in principle, we should use $\hat{Q}(q+\delta q)$ in Eq. (36) instead of $\hat{Q}(q)$, namely the generator at the same point $q + \delta q$. The prescription given in Sec. II C 3 actually approximates the generator $\hat{Q}(q+\delta q)$ by the one at the previous point $\hat{Q}(q)$. The approximation significantly reduces the computational task. This approximation turns out to be very good as far as $\delta q$ is small enough. After moving the state from $|\psi(q)\rangle$ to $|\psi(q+\delta q)\rangle$ with small $\delta q$, the self-consistency can be checked in the following way. At $|\psi(q+\delta q)\rangle$ we calculate the generator $\hat{Q}(q+\delta q)$ by solving the moving RPA equations. Replacing $\hat{Q}(q)$ by $\hat{Q}(q+\delta q)$ in Eq. (36) and changing the constraint condition Eq. (34) to $\langle\psi(q+\delta q)|\hat{Q}(q+\delta q)|\psi(q+\delta q)\rangle = 0$, the self-consistency between $|\psi(q+\delta q)\rangle$ and $\hat{Q}(q+\delta q)$ is guaranteed if the further imaginary-time evolution of Eq. (36) keeps the state $|\psi(q+\delta q)\rangle$ invariant. This is confirmed for the present case. The validity is also confirmed by the fact that the final result is invariant with respect to change of the step size $\delta q$.

#### 4. Summary of the numerical algorithm

We choose the HF ground state as the starting point of the collective path, $|\psi(q=0)\rangle$. The HF ground state is always the solution of Eq. (6) with $\partial V/\partial q = 0$, at which the moving RPA equation becomes identical to the conventional RPA equation. Therefore, without knowing the generator $\hat{Q}(q)$, the starting point $|\psi(q=0)\rangle$ can be determined. The procedure to construct the collective path is given as follows:

(1) Calculate the HF ground state, $|\psi(q=0)\rangle$.
(2) Solve the RPA equation to obtain $\hat{Q}(q=0)$ and $\hat{P}(q=0)$.
(3) When $|\psi(q)\rangle$, $\hat{Q}(q)$, and $\hat{P}(q)$ are provided, solve the moving HF equation to obtain the state $|\psi(q+\delta q)\rangle$, according to the method described in Sec. II C 3.
(4) Solve the moving RPA equation to obtain the generators, $\hat{Q}(q+\delta q)$ and $\hat{P}(q+\delta q)$, according to the method described in Sec. II C 2.
(5) Repeat steps 3 and 4 to determine the collective path.

For step 4 above, we choose the inertial mass $M(q) = 1$. Then, the weak canonicity condition (5) determines the scale of $q$ as

$$2\sum_{mnij} Q_{mi}(q)[A(q) - B(q)]_{minj}Q_{nj}(q) = 1. \tag{40}$$

The scale transformation from $q$ to $R$ is performed by changing the inertial mass according to Eqs. (19) and (22).

#### 5. Algorithm for fully consistent solutions

Since $^8$Be is one of the simplest cases, we also try another method to get the fully self-consistent solutions of the $\hat{P}(q)$, $\hat{Q}(q)$, and $|\psi(q)\rangle$ that simultaneously satisfy Eqs. (6), (7), and (8). For $^8$Be, the conventional constrained calculation on $Q_{20}$ may produce approximate solutions, $|\psi^{(0)}(q)\rangle$. Thus, we adopt $|\psi^{(0)}(q)\rangle$ as the initial trial wave functions, and start the following iteration procedure:

(i) Solve Eqs. (7) and (8) to obtain $(\hat{Q}(q),\hat{P}(q))$, by selecting the quadrupole mode $Q_{20}$.
(ii) Use this $\hat{Q}(q)$ to solve the moving HF equation (6) with the constraint $\langle\psi(q)|\hat{Q}(q)|\psi(q)\rangle = 0$.
(iii) Put the obtained state $|\psi(q)\rangle$ into Eqs. (7) and (8), then go back to step (i).

We also use the initial trial states prepared by the CHF calculation with constraint on the relative distance $\hat{R}$. Although

the initial states $|\psi^{(0)}(q)\rangle$ are different from those obtained with the $\hat{Q}_{20}$ operator, after the iteration of (i)–(iii) converges, they reach the same self-consistent solutions, $|\psi(q)\rangle$ and $(\hat{Q}(q), \hat{P}(q))$.

It should be noted again that the prescription in Sec. II C 3 is significantly easier than the present iteration (i)–(iii). At every point $q$, the self-consistency requires us to solve the moving RPA equations many times to determine the self-consistent state $|\psi(q)\rangle$. We have confirmed that the solution of these iteration procedures (i)–(iii) is practically identical to the one obtained with the algorithm in Sec. II C 3.

## III. NUMERICAL RESULTS

In this work the BKN energy density functional is adopted as a test for the numerical application of the ASCC method. The BKN energy density functional is rather schematic, thus we should take the following results in a qualitative sense.

### A. Results of the RPA calculation at the ground state

If the frequency $\omega$ is positive ($\omega^2 > 0$) for Eq. (13), we may construct the normal-mode excitation operator $\Omega^\dagger(q)$ from the generators $(\hat{Q}(q), \hat{P}(q))$ as

$$\Omega^\dagger(q) = \sqrt{\frac{\omega(q)}{2}}\hat{Q}(q) - \frac{i}{\sqrt{2\omega(q)}}\hat{P}(q). \tag{41}$$

For a Hermitian one-body operator $\hat{D}$, defined by Eq. (4) with replacement of $Q_{nj}(q) \to D_{nj}$, the transition matrix element is given by

$$\begin{aligned}\langle\omega|\hat{D}|0\rangle &\equiv \langle 0|[\Omega(q), \hat{D}]|0\rangle \\ &= \sqrt{\frac{2}{\omega}}\sum_i \int d\vec{r}\; P_i(\vec{r})D_i(\vec{r}).\end{aligned} \tag{42}$$

We assume that, for the coordinate representation of the operator such as $P_i(\vec{r})$ or $D(\vec{r})$, the hole components are always projected out according to Eq. (27). The collective character of the state $|\omega\rangle$ can be identified by choosing the one-body operator $\hat{D}$. For instance, the translational motion along $z$ axis is identified by a sizable transition matrix element of the center-of-mass operator, $\hat{D} = A^{-1}\sum_k^A z_k$. For the relative motion of two $\alpha$ particles, we may choose the mass quadrupole operator (Sec. III A 2).

#### 1. *Translational motion of a single α particle*

First, we show results for the single $\alpha$ particle. In this case, the model space is a sphere of radius $R = 7$ fm with various mesh sizes $h = 0.5$–$1.4$ fm. Note that the ground state of the system is a trivial solution of the ASCC equation (6). We can clearly identify the three translational modes for $x$, $y$, and $z$ directions, degenerated in energy at $\omega_{\rm com} \leqslant 1$ MeV. Using smaller mesh size, the eigenfrequency of the translational motion approaches to zero. There are no low-lying excited states in the $\alpha$ particle because of its compact and doubly closed characters. The calculated energy of the lowest excited state is larger than 20 MeV.

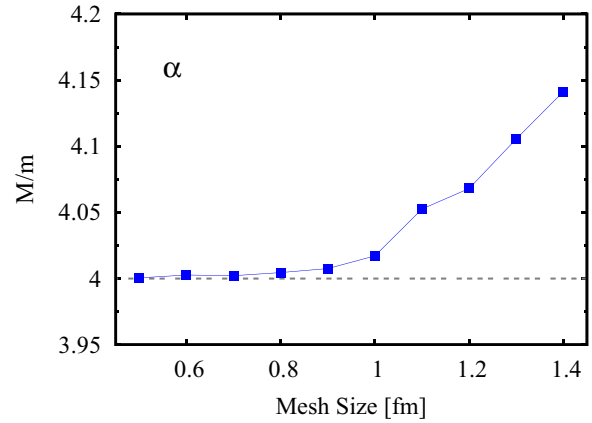


FIG. 1. Calculated translational mass of the $\alpha$ particle in units of the nucleon's mass $m$.

Using Eqs. (19) and (22) with $R$ as the center of mass, we calculate the inertial mass of the translational motion of the $\alpha$ particle. Figure 1 shows the results calculated with different mesh size $h$ of the 3D grid. Since this is the trivial center-of-mass motion of the total system, this should equal the total mass, $M = Am$ with $A = 4$. As the mesh size decreases, the total mass certainly converges to the value of $4m$. In the following, we adopt the mesh size $h = 0.8$ fm.

#### 2. *Relative motion of two α particles in* $^8$Be

Figure 2 shows the calculated eigenfrequencies for the ground state of $^8$Be and the two well separated $\alpha$'s at distance $R = 7.2$ fm. Since the ground state of $^8$Be is deformed, there appear the rotational modes of excitation as the zero modes, in addition to the three independent modes of the translational motion. Because of the axial symmetry of the ground state, the rotation about the symmetry axis ($z$ axis) does not appear. In Fig. 2 the calculation produces two

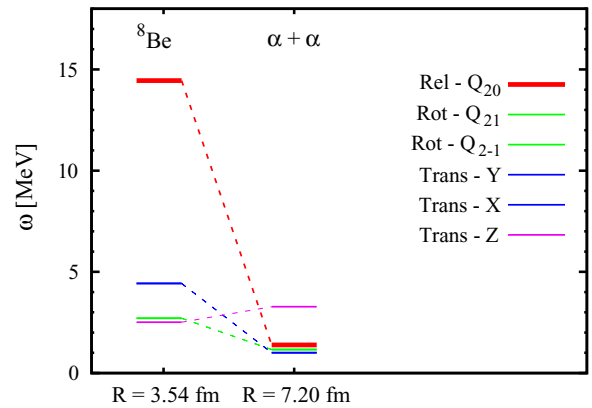


FIG. 2. Calculated eigenfrequencies for the ground state of $^8$Be (left column) and the two well-separated $\alpha$'s at distance $R = 7.2$ fm (right column). The three modes of translational motion and two modes of rotational motion are shown by thin lines, while the thick line indicates the $K = 0$ quadrupole oscillation. The translational motions along the $x$ and the $y$ directions are degenerate in energy, and the same for the rotational motions.

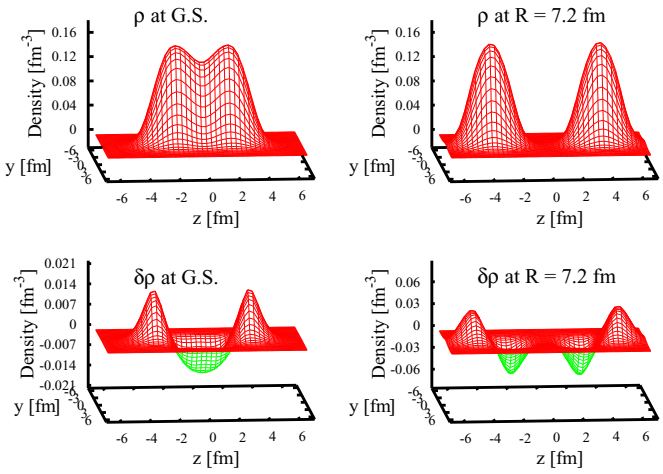


FIG. 3. The density distribution $\rho(\vec{r})$ for $^8$Be in the upper panels and the transition density $\delta\rho(\vec{r})$ of the lowest mode of excitation in the lower panels. The left panels show those at the ground state and the right panels show those at $R = 7.2$ fm. Those on the $y$-$z$ plane are plotted.

rotational modes of excitation around 2.8 MeV with large transition matrix element of the $K = 1$ quadrupole operator, $\hat{Q}_{2\pm1} \equiv \int r^2 Y_{2\pm1}(\hat{r})\hat{\psi}^\dagger(\vec{r})\hat{\psi}(\vec{r})d\vec{r}$. The finite energy of these rotational modes comes from the finite mesh size discretizing the space. Besides these five zero modes, the lowest mode of excitation turns out to have a sizable transition strength of the $K = 0$ quadrupole operator $\hat{Q}_{20} \equiv \int r^2 Y_{20}(\hat{r})\hat{\psi}^\dagger(\vec{r})\hat{\psi}(\vec{r})d\vec{r}$. This mode corresponds to the elongation of $^8$Be. The transition density is given by

$$\delta\rho(\vec{r}) \equiv \langle\omega|\hat{\psi}(\vec{r})\hat{\psi}^\dagger(\vec{r})|0\rangle = \langle 0|\left[\Omega, \hat{\psi}(\vec{r})\hat{\psi}^\dagger(\vec{r})\right]|0\rangle$$
$$= \sqrt{\frac{2}{\omega}} \sum_i P_i(\vec{r})\varphi_i(\vec{r}). \tag{43}$$

The left panels of Fig. 3 show the density profile of $^8$Be and the transition density $\delta\rho(r)$ corresponding to the lowest RPA normal mode. We can see an elongated structure along the $z$ direction in the ground state. The lowest mode of excitation corresponds to the change of its elongation ($\beta$ vibration).

We also perform the same calculation for the state in which two $\alpha$ particles are located far away, at the relative distance $R = 7.2$ fm. In the right panel of Fig. 3, we clearly see that the two $\alpha$ particles are well separated, and the quadrupole mode in fact corresponds to the translational motion of the $\alpha$ particles in opposite directions; namely, the relative motion of two $\alpha$'s. The excitation energy almost vanishes for this normal mode (Fig. 2).

### B. Results of the ASCC method

In Sec. III A 2, we show that the the lowest quadrupole mode of excitation at the ground state of $^8$Be may change its character and lead to the relative motion of two $\alpha$'s at the asymptotic region. We adopt this mode as the generators $(\hat{Q}(q), \hat{P}(q))$ of the collective variables $(q, p)$, then we construct the collective path.

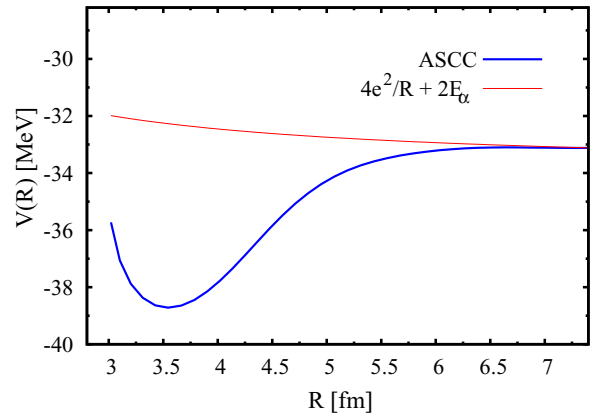


FIG. 4. Potential energy as a function of the relative distance $R$. The solid (blue) line corresponds to $V(R)$ on the ASCC collective path, while the dashed (red) line shows $4e^2/R + 2E_\alpha$ for reference.

#### 1. Collective path, potential, and inertial mass

We successfully derive the collective path $\{|\psi(q)\rangle;\ q = 0, \delta q, 2\delta q, \ldots\}$ connecting the ground state of $^8$Be into the well-separated two $\alpha$ particles. The inertial mass $M(q)$ is taken as unity and the collective potential is calculated according to Eq. (9). Then, according to Sec. II B, the collective coordinate $q$ is mapped onto the relative distance $R \equiv \langle\psi(q)|\hat{R}|\psi(q)\rangle$ with Eq. (18). Figure 4 shows the obtained potential energy along the ASCC collective path. As a reference, we also show the pure Coulomb potential between two $\alpha$ particles at distance $R$, $4e^2/R + 2E_\alpha$, where $E_\alpha$ is the calculated ground state energy of the isolated $\alpha$ particle. Apparently, it asymptotically approaches the pure Coulomb potential. As two $\alpha$'s get closer, the potential starts to deviate from the Coulomb potential at $R < 6$ fm and finally reaches the ground state of $^8$Be. The ground state is at $R = 3.54$ fm, and the top of the Coulomb barrier is at $R = 6.6$ fm. Note that the path is determined self-consistently without any *a priori* assumption.

With this calculated potential, we may check the self-consistency of the ASCC potential and the eigenfrequency. If the collective path perfectly follows the direction defined by the local generators $(\hat{Q}(p), \hat{P}(q))$ at each point of $q$, the second derivative of the potential $d^2V/dq^2$ should coincide with the eigenfrequency $\omega^2$ of the moving RPA equation. The almost perfect agreement between these is shown in Fig. 5.

For the region of $R < 3.5$ fm, there exists some discrepancy between $d^2V/dq^2$ and $\omega^2$. In this region, the $^8$Be nucleus has even more compact shapes than the ground state; then, the coordinates $q$ and $R$ become almost orthogonal to each other, losing the one-to-one correspondence between them. In other words, the states $|\psi(q)\rangle$ change as $q$ gets smaller, but keep $R = \langle\psi(q)|\hat{R}|\psi(q)\rangle$ almost constant. In addition, the moving RPA frequency $\omega$ becomes larger than the particle threshold energy, entering in the continuum. Thus, in this region of $R <$ 3.5 fm, the results somewhat depend on the adopted box size.

Figure 6 shows the obtained inertial mass $M(R)$ as a function of $R$ for the scattering between two $\alpha$'s As the two $\alpha$'s are far away, the ASCC inertial mass asymptotically produces the exact reduced mass of $2m$. This means that the collective coordinate $q$ becomes parallel to the relative distance $R$, even

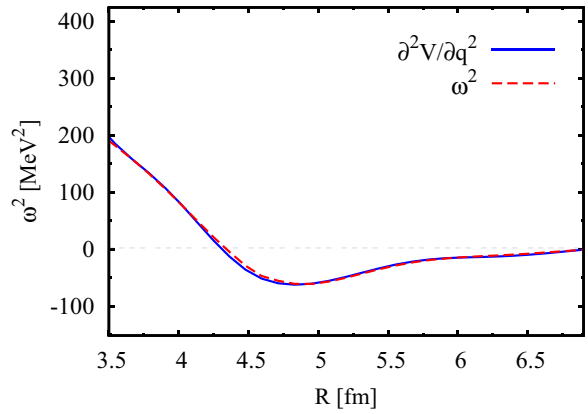


FIG. 5. $\omega^2$ in Though we do not assume so. At $R < 3.54$ fm, the value of inertial mass $M(R)$ increases. This is due to the decrease of the factor $dR/dq$ in Eq. (19). Making the system even more compact than the ground state, $M(R)$ rises up drastically, which means that the coordinates $q$ and $R$ become almost orthogonal.

### 2. *Phase shift for α-α scattering*

The ASCC calculation provides us the collective Hamiltonian along the optimal reaction path. Using this, we demonstrate the calculation of nuclear phase shift. We should take this result in a qualitative sense, because of a schematic nature of the BKN energy density functional.

Using the collective potential $V(R)$ and the inertial mass $M(R)$ obtained in the ASCC calculation, the nuclear phase shift for the angular momentum $L$ at incident energy $E$ is calculated in the WKB approximation as [42,43]

$$\delta_L(E) = \int_{R_0}^{\infty} k(R)dR - \int_{R_c}^{\infty} k_c(R)dR, \tag{44}$$

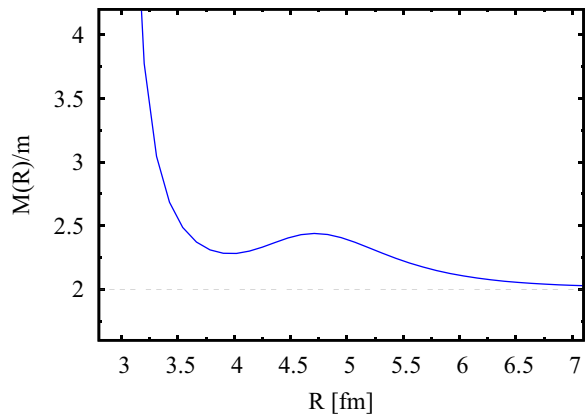


FIG. 6. Inertial mass in units of the nucleon's mass $m$ for the collective path of $\alpha + \alpha \leftrightarrow {}^8$Be, as a function of the relative distance $R$.

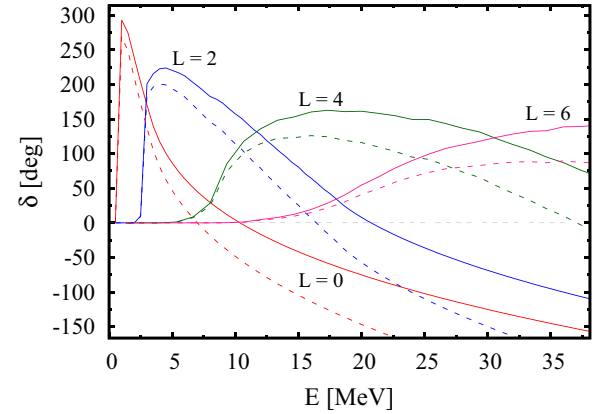


FIG. 7. Nuclear phase shift for the scattering between two $\alpha$ particles, as a function of incident energy $E$. The solid lines indicate the results obtained with the ASCC inertial mass $M(R)$, while the dashed lines are calculated with the constant reduced mass $2m$.

with

$$k^2(R) = 2M(R)\left\{E - V(R) - \frac{\left(L+\frac{1}{2}\right)^2}{4mR^2}\right\},$$
$$k_c^2(R) = 4m\left\{E - \frac{4e^2}{R} - \frac{\left(L+\frac{1}{2}\right)^2}{4mR^2}\right\}, \tag{45}$$

where $k(R)$ and $k_c(R)$ are the wave numbers in the radial motion with and without the nuclear potential. $R_0$ and $R_c$ are the outer turning points for the potentials $V(R)$ and $4e^2/R$, respectively, i.e., $k(R_0) = k_c(R_c) = 0$. The centrifugal potential is approximated as $(L+1/2)^2/(2\mu R^2)$ with the reduced mass $\mu = 2m$ and the semiclassical approximation for $L(L+1)$. We assume $V(R) = +\infty$ for $R < 3$ fm in which the obtained optimal reaction path is almost orthogonal to $R$.

Figure 7 shows the calculated nuclear phase shifts for the scattering between two $\alpha$'s. The dashed line is calculated with the same potential $V(R)$ but with the constant reduced mass, $M(R) \to \mu = 2m$. We can see the prominent increase of the nuclear phase shift caused by the coordinate-dependent ASCC inertial mass $M(R)$. We should remark that the energy of the resonance in $^8$Be is not reproduced with the BKN energy density functional. In fact, the present calculation leads to the stable ground state for $^8$Be: $E(^8\text{Be}) < 2E_\alpha$. Thus, we should regard this result as a qualitative one. Nevertheless, the basic features of phase shifts for the $\alpha$-$\alpha$ scattering are roughly reproduced. This demonstrates the usefulness of the requantization using the ASCC calculation.

## C. Comparison with other approaches

We compare the present ASCC results with those obtained with other approaches: (i) CHF + cranking inertia, (ii) CHF + local RPA, and (iii) ATDHF. We adopt the same model space as the ASCC calculations for these calculations. For the constraint operators of the CHF calculation in (i) and (ii), we adopt the $K = 0$ mass quadrupole operator $\hat{Q}_{20}$ and the relative distance $\hat{R}$.

### 1. CHF + cranking inertia

Since $^8$Be is the simplest system and has a prominent $\alpha+\alpha$ structure even at the ground state, the collective path can be approximated by more conventional CHF calculations with a constraint operator as either $\hat{Q}_{20}$ or $\hat{R}$. The potential is defined as $V_{\rm CHF}(R)=\langle\psi_{\rm CHF}(R)|\hat{H}|\psi_{\rm CHF}(R)\rangle$. For the inertial mass, Inglis's cranking formula is widely used. There are two kinds of cranking formulas: The original formula is derived by the adiabatic perturbation, which is given for the 1D collective motion as

$$M^{\rm NP}_{\rm cr}(R)=2\sum_{m,i}\frac{|\langle\varphi_m(R)|\partial/\partial R|\varphi_i(R)\rangle|^2}{e_m(R)-e_i(R)}, \tag{46}$$

where the single-particle states and energies are defined with respect to $h_{\rm CHF}(R)=h_{\rm HF}[\rho]-\lambda(R)\hat{O}$ as

$$h_{\rm CHF}(R)|\varphi_\mu(R)\rangle=e_\mu(R)|\varphi_\mu(R)\rangle,\quad \mu=i,m. \tag{47}$$

Note that, depending on choice of the constraint operator, $\hat{O}=(\hat{Q}_{20},\hat{R})$, we obtain slightly different $|\varphi_i(R)\rangle$ even at the same $R$.

Another formula, which is more frequently used in many applications and also called the cranking inertial mass, is derived, by assuming the separable interaction and taking the adiabatic limit of the RPA inertial mass,

$$M^{\rm P}_{\rm cr}(R)=\frac{1}{2}\{S^{(1)}(R)\}^{-1}S^{(3)}(R)\{S^{(1)}(R)\}^{-1}, \tag{48}$$

with

$$S^{(k)}(R)=\sum_{m,i}\frac{|\langle\varphi_m(R)|\hat{R}|\varphi_i(R)\rangle|^2}{\{e_m(R)-e_i(R)\}^k}. \tag{49}$$

The residual fields induced by the density fluctuation is neglected in both of these cranking formulas. According to Ref. [44], we call the former one in Eq. (46) "nonperturbative" cranking inertia and the latter in Eq. (48) "perturbative" one. The method of CHF + cranking inertia has been widely used for many applications, including studies of nuclear structure [45–53] and fission dynamics [44,54,55].

The obtained potentials with different constraint operators are shown in Fig. 8. The two constraints $\hat{Q}_{20}$ and $\hat{R}$ give very similar potential surfaces, which is also close to the ASCC result. On the other hand, the inertial masses are more sensitive to the difference. In Fig. 9, we show the perturbative and nonperturbative cranking inertial masses based on the states obtained with CHF calculations with different constraint operators. We include all the single-particle states in the model space for the calculation of Eqs. (46) and (49). They present significant variations, especially in the region where two $\alpha$'s stick together into one nucleus. First of all, they are larger than the ASCC inertia. Second, the non-perturbative and perturbative cranking inertial masses are significantly different. For instance, the calculations with $\hat{Q}_{20}$ constraint suggest prominent peak structure in $M^{\rm NP(P)}_{\rm cr}(R)$. However, the peak positions are very different. It should be noted that the present results should not be generalized to other energy density functionals, because the BKN energy density functional has no time-odd mean fields [see Eq. (24)].

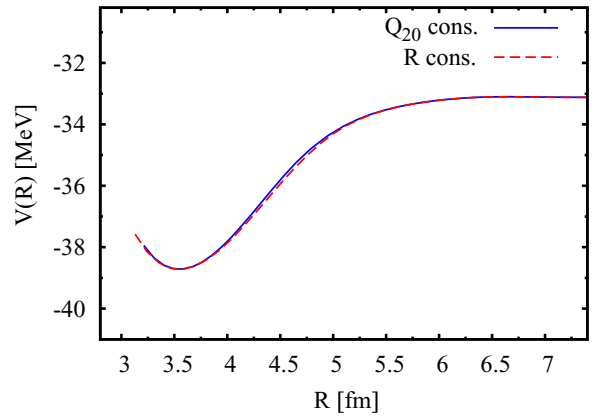


FIG. 8. The collective potential obtained with the CHF calculation. The solid (blue) and dashed (red) lines indicate the results with constraints on $\hat{Q}_{20}$ and $\hat{R}$, respectively.

Since there are neither effective mass nor time-odd mean field in the BKN energy density functional, we expect that in the asymptotic region the exact translational mass $Am$ can be reproduced. This turns out to be true for $M^{\rm NP}_{\rm cr}(R)$, which reduces to the exact value $2m$, while $M^{\rm P}_{\rm cr}(R)$ approaches $2m$ much slower than $M^{\rm NP}_{\rm cr}(R)$ and might converge to a larger value. In fact, for a single $\alpha$ particle, the translational mass is calculated as $M^{\rm P}_{\rm cr}=4.16m$. The same kind of deviation is presented in the asymptotic value of the reduced mass in Fig. 9.

### 2. CHF + local RPA

The cranking inertial mass has known weak points: namely, missing residual correlations and an adiabatic assumption. The problem becomes particularly serious when the time-odd mean fields play a role as residual fields. Although the BKN energy density functional adopted in this paper does not have the time-odd components, it may be useful to investigate the significance of the residual effect.

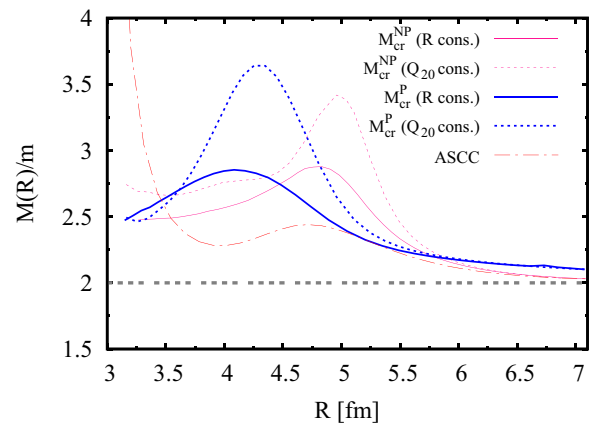


FIG. 9. Cranking inertial mass based on the CHF state. The solid and dashed lines indicate the results with constraints on $\hat{R}$ and $\hat{Q}_{20}$, respectively. The nonperturbative and perturbative cranking inertial masses are shown with thin and thick lines, respectively.

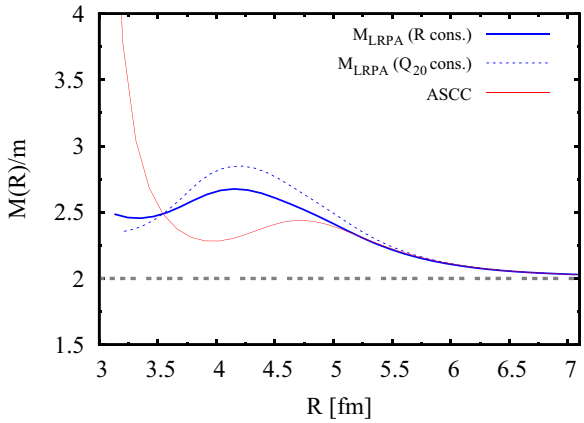


FIG. 10. Inertial mass calculated with the CHF + local RPA method in units of nucleon's mass. The solid and dashed lines indicate the results with constraints on $\hat{R}$ and $\hat{Q}_{20}$, respectively. The ASCC result is shown by the thin line for comparison.

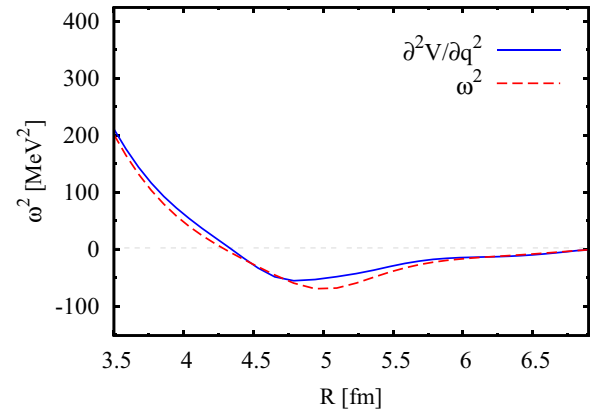


FIG. 11. $\omega^2$ in Eq. (13) and $\partial^2 V/\partial q^2$ of the CHF + local RPA calculation.

In order to take into account the residual effect, we adopt the method called "CHF + local RPA". This is defined by replacing $\hat{H}_{\rm mv}(q)$ in the ASCC equations (6), (7), and (8), with the constrained Hamiltonian, $\hat{H}' \equiv \hat{H} - \lambda \hat{O}$, where $\hat{O}$ is an adopted constraint operator. In other words, the collective path is defined by hand, but the inertial mass is defined by the RPA equations with $\hat{H}'$. The calculated inertial mass $M_{\rm lrpa}(q)$ for the motion along the coordinate $q$, can be mapped onto the variable $R$, $M_{\rm lrpa}(R)$, assuming a one-to-one correspondence exists between $q$ and $R$. This is done exactly in the same way as the ASCC (Sec. II B). However, the consistency between the generators, $\hat{Q}(q)$ and $\hat{P}(q)$, and the collective path $\{|\psi(q)\rangle\}$ is lost. This method of CHF + local RPA has been applied to studies of nuclear structure with the separable Hamiltonian [22–25,56,57].

In Fig. 10, we show the result of the local RPA calculation based on the CHF states. At the ground state ($R = 3.54$ fm), since both the CHF + local RPA and the ASCC calculations reduce to the HF + RPA calculation, they produce identical inertial masses. $M_{\rm lrpa}(R)$ also converges to the ASCC value at large $R$, faster than $M_{\rm cr}^{\rm NP}(R)$, and asymptotically gives the exact reduced mass $2m$. Especially, the calculation with the $R$ constraint produces almost identical results as the ASCC method, at $R > 5$ fm.

The self-consistency between the local generators and the assumed coordinate can be checked by comparing the local RPA frequency and the second derivative of the potential $V(R)$. If they are consistent, we expect the relation

$$\omega^2 = \frac{d^2V}{dq^2} = \frac{d^2V}{dR^2}\frac{1}{M_{\rm lrpa}(R)} + \frac{dV}{dR}\frac{d^2R}{dq^2}. \tag{50}$$

It turns out that the last term is negligible. Taking the potential $V(R)$ of the $Q_{20}$ constrained calculation as an example, this comparison is shown in Fig. 11. We can see some deviations in the region of $3.5 < R < 6$ fm, although the overall agreement is not so bad. The deviation indicates that the CHF states are not exactly on the collective path defined by the local generators $(\hat{Q}(R), \hat{P}(R))$. On the other hand, perfect agreement is seen in the region $R > 6$ fm. This suggests that, at $R > 6$ fm, the optimal collective coordinate $q$ obtained with the ASCC method coincides with the relative distance $R$ and the quadrupole moment $Q_{20}$.

Finally, we remark on the necessity of modifying the constraint operators, such as $\hat{Q}_{20}$ and $\hat{R}$, in the CHF calculation. Taking the constraint operator $\hat{Q}_{20}$ as an example, on the symmetry axis ($z$ axis), the constraint term $-\lambda \hat{Q}_{20}$ results in a external potential proportional to $-z^2$. If we adopt a large model space, the CHF calculation may lead to an unphysical solution, namely, the appearance of small density at the edge of the box. In order to avoid these unphysical states, we have to screen the operator in the outer region: $\tilde{Q}_{20} \equiv \int f(r) r^2 Y_{20}(\hat{r}) \hat{\psi}^\dagger(\vec{r}) \hat{\psi}(\vec{r}) d\vec{r}$ with a screening function $f(r)$ which should be unity in the relevant region and vanish in the irrelevant region ($r > R_0$). The function form of $f(r)$ becomes nontrivial when two nuclei are far away in an asymptotic region. This kind of complication is not necessary for the ASCC local generator $\hat{Q}(q)$, because it vanishes in a region where all the hole orbits are zero $\varphi_i(\vec{r}; q) = 0$. In other words, the ASCC generators are properly "screened" automatically.

### 3. ATDHF

The ATDHF is based on Eqs. (6) and (7). Since the second-order equation (8) is missing, the collective path is not unique. We follow the prescriptions given in Ref. [58] for practical calculations. The equation of the collective path is formulated in a form of the first-order differential equation for $|\psi(q)\rangle$,

$$\frac{\partial}{\partial q}|\psi(q)\rangle = \frac{M_{\rm atdhf}(q)}{dV/dq}[\hat{H}, \hat{H}_{\rm ph}]_{\rm ph}|\psi(q)\rangle, \tag{51}$$

where $\hat{H}_{\rm ph}$ is the ph and hp parts of the Hamiltonian defined locally at each $q$. The single-particle wave functions $|\varphi_i(q)\rangle$ in the Slater determinant $|\psi(q)\rangle$ is evolved according to the following equation:

$$|\varphi_i(q-\delta q)\rangle = |\varphi_i(q)\rangle - \varepsilon\{1-\rho(q)\}(h_{\rm HF}(q)\{1-2\rho(q)\}h_{\rm HF}(q) + {\rm Tr}\{v[h_{\rm HF}(q), \rho(q)]\})|\varphi_i(q)\rangle \tag{52}$$

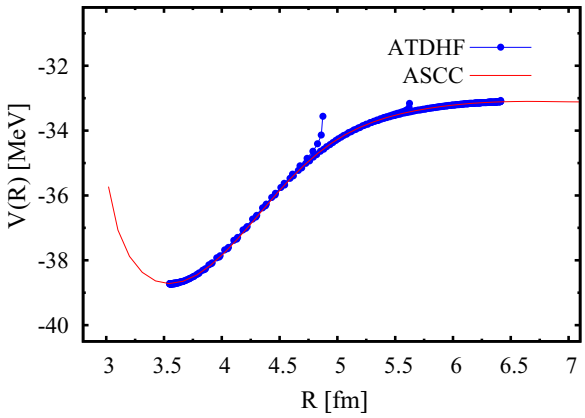


FIG. 12. The potential energy on the ATDHF collective path derived by Eq. (52), as a function of relative distance $R$. Initial distances between the two $\alpha$ particles are set to be $R = 4.8$,5.6,6.4 fm respectively. The thin (red) line indicates the result of the ASCC method.

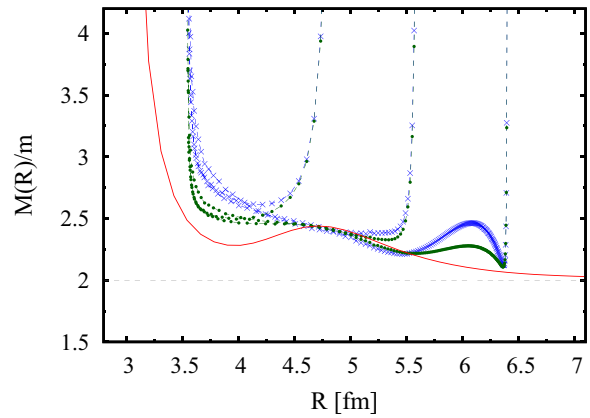


FIG. 13. $M_{\rm atdhf}(R)$ calculated by Eqs. (56) and (57) shown with blue crosses and green dots, respectively. They are based on the same ATDHF trajectories in Fig. 12. The solid (red) line indicates the ASCC mass for comparison.

with

$$\varepsilon = \frac{\delta q M_{\rm atdhf}(q)}{dV/dq}. \tag{53}$$

In order to obtain the stable solutions, $\varepsilon$ is set to be a small real number. Successive application of Eq. (52) gives the ATDHF collective path. Solutions with different initial conditions of $|\psi(0)\rangle$ produce different collective paths. The envelope curve of all these trajectories is regarded as the final solution of the adiabatic collective path.

The ATDHF inertial mass is given by

$$M_{\rm atdhf}(q) = \langle\psi(q)|[\hat{Q}(q),[\hat{H},\hat{Q}(q)]]|\psi(q)\rangle^{-1}, \tag{54}$$

with

$$\hat{Q}(q) = \left(\frac{\partial V}{\partial q}\right)^{-1}\hat{H}_{\rm ph}(q) = \left(\frac{\partial V}{\partial q}\right)^{-1}\{h_{\rm HF}(q)\}_{\rm ph}. \tag{55}$$

According to Eq. (19), the mass with respect to the relative distance $R$ can be calculated as

$$\begin{aligned} M_{\rm atdhf}(R) &= M_{\rm atdhf}(q)\left(\frac{dq}{dR}\right)^2 \\ &= \left(\frac{dV}{dR}\right)^2\langle\psi(q)|[\hat{H}_{\rm ph}(q),[\hat{H},\hat{H}_{\rm ph}(q)]]|\psi(q)\rangle^{-1}. \end{aligned} \tag{56}$$

Another, even easier, way of calculating $M_{\rm atdhf}(R)$ is simply inverting Eq. (53). Using Eqs. (19) and (53), we obtain

$$M_{\rm atdhf}(R) = \left(\frac{dq}{dR}\right)^2\frac{\varepsilon}{\delta q}\frac{dV}{dq} = \frac{\varepsilon}{\delta R}\frac{dV}{dR}. \tag{57}$$

For the scattering between two $\alpha$'s, we prepare two $\alpha$ particles both at ground states separately, then put them at different distances of $R = 4.8$, 5.6, 6.4 fm, as the initial conditions for Eq. (52). The potential surface of the ATDHF trajectories is plotted in Fig. 12, which shows how the solutions of Eq. (51) with different initial conditions converge to a common collective path. The converged ATDHF potential surface is similar to the potentials of CHF and ASCC calculations. It should be noted that we can obtain these fall-line trajectories on the potential surface which go only from high to low energy [58]. It becomes numerically unstable if we calculate in the opposite direction. Thus, we cannot start from the HF ground state, and it is difficult to obtain the solution in a region of $R < 3.5$ fm, beyond the HF minimum state.

Figure 13 shows the mass parameters based on the same trajectories in Fig. 12. The inertial masses calculated with Eqs. (56) and (57) roughly produce the identical results. Near the HF state of $R = 3.54$ fm, the inertial mass increases drastically. This is very different from the result of the former calculations [15,58], the reason of which is currently under investigation. We also encounter a difficulty to obtain the collective path in the asymptotic region at large $R$. A larger model space and finer mesh size seems to be needed to obtain the potential in the asymptotic region and to reproduce the reduced mass $2m$. We should also mention that the saddle point with $dV/dR = 0$ is extremely difficult to reach by solving Eq. (52). In the ASCC method, we do not encounter these difficulties, and are able to obtain the unique reaction path and inertial mass.

## IV. SUMMARY

We applied the ASCC method to the determination of the nuclear reaction path, the collective potential, and the collective inertial mass. The 3D coordinate space representation is adopted for the single-particle wave functions. Using the imaginary-time method and the finite-amplitude method, the coupled equations of the ASCC, that consist of the moving HF equation and the moving RPA equations, are solved iteratively. The generators are represented in the mixed representation of the hole orbit and the coordinate grid points, such as $Q_j(\vec{r})$.

The first application was performed for the simplest case, the scattering of $\alpha + \alpha \leftrightarrow {}^8$Be. The reaction path, the poten-

tial, and the inertial mass were successfully determined. Even though the system is too simple to expect significant difference in the reaction path, a comparison with the cranking inertial mass demonstrates some advantages of the ASCC method. In particular, the cranking inertial mass is very sensitive to the adopted prescription of perturbative or nonperturbative formulas. The perturbative cranking mass seems not to reduce to the exact value of the reduced mass at $R \to \infty$. For $^{8}$Be, the potential does not depend on the choice of the constraint operator. In contrast, a proper choice of the operator is important for the inertial mass. The ASCC method is able to remove these ambiguities and provide improvement of the cranking formula. The ATDHF theory is an alternative way to derive the reaction path and inertial mass. However, we have found that finding the unique converged result of the ATDHF trajectories is significantly more difficult than the ASCC method.

The reaction path and the feature of the inertial mass depend on the reaction system. The calculation for heavier systems is in progress. With the techniques presented in this work, it is feasible to perform the calculation of the inertial mass for different modes of nuclear collective motion, such as the rotational moment of inertia, and the mass parameter for different vibrational modes. The lowest mode of excitation changes from nucleus to nucleus, and we will investigate how these nuclear excitation properties influence the reaction dynamics.

The simple BKN energy density functional should be replaced by a modern nuclear energy density functional, in future. The presence of time-odd mean fields would significantly affect dynamical behaviors of nuclear systems. Since the cranking inertia cannot take into account the time-odd effects, advantages of the ASCC method become even clearer. The inclusion of the paring correlation is another important issue. This has been studied in nuclear structure problems [3]. However, for the nuclear reaction studies, some conceptual problems for the paired systems still remain to be solved. For instance, the ASCC method for the reaction of two nuclei with different chemical potentials has not been established yet. This is also an important subject for future efforts.

## ACKNOWLEDGMENTS

This work is supported in part by JSPS KAKENHI Grants No. 25287065 and by ImPACT Program of the Council for Science, Technology and Innovation (Cabinet Office, Government of Japan).

[1] J. W. Negele, Rev. Mod. Phys. **54**, 913 (1982).
[2] C. Simenel, Eur. Phys. J. A **48**, 1 (2012).
[3] T. Nakatsukasa, K. Matsuyanagi, M. Matsuo, and K. Yabana, Rev. Mod. Phys. **88**, 045004 (2016).
[4] T. Nakatsukasa, Prog. Theor. Exp. Phys. (2012) 01A207.
[5] J. A. Maruhn, P.-G. Reinhard, P. D. Stevenson, and A. S. Umar, Comput. Phys. Commun. **185**, 2195 (2014).
[6] P. Ring and P. Schuck, *The Nuclear Many-Body Problems*, Texts and Monographs in Physics (Springer-Verlag, New York, 1980).
[7] J.-P. Blaizot and G. Ripka, *Quantum Theory of Finite Systems* (MIT Press, Cambridge, MA, 1986).
[8] H. Reinhardt, Nucl. Phys. A **346**, 1 (1980).
[9] M. Baranger, M. Strayer, and J.-S. Wu, Phys. Rev. C **67**, 014318 (2003).
[10] D. M. Brink, M. J. Giannoni, and M. Veneroni, Nucl. Phys. A **258**, 237 (1976).
[11] F. Villars, Nucl. Phys. A **285**, 269 (1977).
[12] M. Baranger and M. Véneroni, Ann. Phys. (N.Y.) **114**, 123 (1978).
[13] K. Goeke and P.-G. Reinhard, Ann. Phys. (N.Y.) **112**, 328 (1978).
[14] P.-G. Reinhard and K. Goeke, Nucl. Phys. A **312**, 121 (1978).
[15] K. Goeke, F. Grümmer, and P.-G. Reinhard, Ann. Phys. (N.Y.) **150**, 504 (1983).
[16] P.-G. Reinhard and K. Goeke, Rep. Prog. Phys. **50**, 1 (1987).
[17] T. Marumori, T. Maskawa, F. Sakata, and A. Kuriyama, Prog. Theor. Phys. **64**, 1294 (1980).
[18] M. Matsuo, Prog. Theor. Phys. **76**, 372 (1986).
[19] M. Matsuo, T. Nakatsukasa, and K. Matsuyanagi, Prog. Theor. Phys. **103**, 959 (2000).
[20] N. Hinohara, T. Nakatsukasa, M. Matsuo, and K. Matsuyanagi, Prog. Theor. Phys. **119**, 59 (2008).
[21] N. Hinohara, T. Nakatsukasa, M. Matsuo, and K. Matsuyanagi, Phys. Rev. C **80**, 014305 (2009).
[22] N. Hinohara, K. Sato, T. Nakatsukasa, M. Matsuo, and K. Matsuyanagi, Phys. Rev. C **82**, 064313 (2010).
[23] N. Hinohara, K. Sato, K. Yoshida, T. Nakatsukasa, M. Matsuo, and K. Matsuyanagi, Phys. Rev. C **84**, 061302 (2011).
[24] N. Hinohara, Z. P. Li, T. Nakatsukasa, T. Nikšić, and D. Vretenar, Phys. Rev. C **85**, 024323 (2012).
[25] K. Sato, N. Hinohara, K. Yoshida, T. Nakatsukasa, M. Matsuo, and K. Matsuyanagi, Phys. Rev. C **86**, 024316 (2012).
[26] K. Matsuyanagi, M. Matsuo, T. Nakatsukasa, K. Yoshida, N. Hinohara, and K. Sato, J. Phys. G: Nucl. Part. Phys. **43**, 024006 (2016).
[27] A. Mukherjee and M. Pal, Nucl. Phys. A **373**, 289 (1982).
[28] A. Klein, N. R. Walet, and G. D. Dang, Ann. Phys. (N.Y.) **208**, 90 (1991).
[29] K. Davies, H. Flocard, S. Krieger, and M. Weiss, Nucl. Phys. A **342**, 111 (1980).
[30] T. Nakatsukasa, T. Inakura, and K. Yabana, Phys. Rev. C **76**, 024318 (2007).
[31] P. Avogadro and T. Nakatsukasa, Phys. Rev. C **84**, 014314 (2011).
[32] P. Avogadro and T. Nakatsukasa, Phys. Rev. C **87**, 014331 (2013).
[33] N. Hinohara, T. Nakatsukasa, M. Matsuo, and K. Matsuyanagi, Prog. Theor. Phys. **117**, 451 (2007).
[34] W. Pauli, *Handbuch der Physik*, Vol. XXIV (Springer Verlag, Berlin, 1933).
[35] P. Bonche, S. Koonin, and J. W. Negele, Phys. Rev. C **13**, 1226 (1976).

[36] M. Stoitsov, M. Kortelainen, T. Nakatsukasa, C. Losa, and W. Nazarewicz, Phys. Rev. C **84**, 041305 (2011).
[37] H. Liang, T. Nakatsukasa, Z. Niu, and J. Meng, Phys. Rev. C **87**, 054310 (2013).
[38] N. Hinohara, M. Kortelainen, and W. Nazarewicz, Phys. Rev. C **87**, 064309 (2013).
[39] T. Nikšić, N. Kralj, T. Tutiš, D. Vretenar, and P. Ring, Phys. Rev. C **88**, 044327 (2013).
[40] J. C. Pei, M. Kortelainen, Y. N. Zhang, and F. R. Xu, Phys. Rev. C **90**, 051304 (2014).
[41] M. Kortelainen, N. Hinohara, and W. Nazarewicz, Phys. Rev. C **92**, 051302 (2015).
[42] D. Brink, *Semi-Classical Methods for Nucleus-Nucleus Scattering* (Cambridge University Press, Cambridge, UK, 1985).
[43] M. Saraceno, P. Kramer, and F. Fernandez, Nucl. Phys. A **405**, 88 (1983).
[44] A. Baran, J. A. Sheikh, J. Dobaczewski, W. Nazarewicz, and A. Staszczak, Phys. Rev. C **84**, 054321 (2011).
[45] M. Baranger and K. Kumar, Nucl. Phys. A **110**, 490 (1968).
[46] M. Baranger and K. Kumar, Nucl. Phys. A **122**, 241 (1968).
[47] E. K. Yuldashbaeva, J. Libert, P. Quentin, and M. Girod, Phys. Lett. B **461**, 1 (1999).
[48] L. Próchniak and S. G. Rohoziński, J. Phys. G: Nucl. Part. Phys. **36**, 123101 (2009).
[49] T. Nikšić, Z. P. Li, D. Vretenar, L. Próchniak, J. Meng, and P. Ring, Phys. Rev. C **79**, 034303 (2009).
[50] Z. P. Li, T. Nikšić, D. Vretenar, J. Meng, G. A. Lalazissis, and P. Ring, Phys. Rev. C **79**, 054301 (2009).
[51] J. P. Delaroche, M. Girod, J. Libert, H. Goutte, S. Hilaire, S. Péru, N. Pillet, and G. F. Bertsch, Phys. Rev. C **81**, 014303 (2010).
[52] Z. P. Li, T. Nikšić, D. Vretenar, P. Ring, and J. Meng, Phys. Rev. C **81**, 064321 (2010).
[53] Z. P. Li, J. M. Yao, D. Vretenar, T. Nikšić, H. Chen, and J. Meng, Phys. Rev. C **84**, 054304 (2011).
[54] M. Warda, J. L. Egido, L. M. Robledo, and K. Pomorski, Phys. Rev. C **66**, 014310 (2002).
[55] J. Sadhukhan, K. Mazurek, A. Baran, J. Dobaczewski, W. Nazarewicz, and J. A. Sheikh, Phys. Rev. C **88**, 064314 (2013).
[56] K. Yoshida and N. Hinohara, Phys. Rev. C **83**, 061302 (2011).
[57] K. Sato and N. Hinohara, Nucl. Phys. A **849**, 53 (2011).
[58] P. G. Reinhard, J. Maruhn, and K. Goeke, Phys. Rev. Lett. **44**, 1740 (1980).